Title

Real-time imaging of Toxoplasma-infected human monocytes under fluidic shear stress reveals rapid translocation of intracellular parasites across endothelial barriers

Journal

Cellular Microbiology, 16(4)

ISSN

1462-5814

Authors

Ueno, Norikiyo
Harker, Katherine S
Clarke, Elizabeth V
et al.

Publication Date

2014-04-01

DOI

10.1111/cmi.12239

Peer reviewed

Published in final edited form as:
Cell Microbiol. 2014 April ; 16(4): 580–595. doi:10.1111/cmi.12239.

Real-time imaging of *Toxoplasma*-infected human monocytes under fluidic shear stress reveals rapid translocation of intracellular parasites across endothelial barriers

Norikiyo Ueno[1], **Katherine S. Harker**[1], **Elizabeth V. Clarke**[1], **Frances Y. McWhorter**[2], **Wendy F. Liu**[2], **Andrea J. Tenner**[1], and **Melissa B. Lodoen**[1,*]

[1]Department of Molecular Biology and Biochemistry and the Institute for Immunology, University of California, Irvine, California, United States of America

[2]Departments of Biomedical Engineering and Chemical Engineering and Material Science and the Edwards Lifesciences Center for Advanced Cardiovascular Technology, University of California, Irvine, California, United States of America

Summary

Peripheral blood monocytes are actively infected by *Toxoplasma gondii* and can function as "Trojan horses" for parasite spread in the bloodstream. Using dynamic live-cell imaging, we visualized the transendothelial migration (TEM) of *T. gondii*-infected primary human monocytes during the initial minutes following contact with human endothelium. On average, infected and uninfected monocytes required only 9.8 and 4.1 minutes, respectively, to complete TEM. Infection increased monocyte crawling distances and velocities on endothelium, but overall TEM frequencies were comparable between infected and uninfected cells. In the vasculature, monocytes adhere to endothelium under the conditions of shear stress found in rapidly flowing blood. Remarkably, the addition of fluidic shear stress increased the TEM frequency of infected monocytes 4.5-fold compared to static conditions (to 45.2% from 10.3%). Infection led to a modest increase in expression of the high affinity conformation of the monocyte integrin Mac-1, and Mac-1 accumulated near endothelial junctions during TEM. Blocking Mac-1 inhibited the crawling and TEM of infected monocytes to a greater degree than uninfected monocytes, and blocking the Mac-1 ligand, ICAM-1, dramatically reduced crawling and TEM for both populations. These findings contribute to a greater understanding of parasite dissemination from the vasculature into tissues.

Introduction

Toxoplasma gondii is an intracellular apicomplexan parasite that infects virtually all warm-blooded animals. Transmission to humans typically occurs by ingestion of parasite tissue cysts or oocysts in contaminated food or water. During acute infection, the bradyzoites or sporozoites within these cysts differentiate into the rapidly dividing tachyzoite form that

*Corresponding author: Melissa B. Lodoen, 3238 McGaugh Hall, Irvine, CA 92697, tel: (949) 824-7805, fax: (949) 824-8551, mlodoen@uci.edu.

The authors have no conflict of interest to declare.

spreads throughout the body (Montoya and Liesenfeld, 2004). Successful dissemination from the intestine to distal organs occurs due to the parasite's ability to cross a wide range of cellular barriers (Barragan and Sibley, 2003), including intestinal epithelium (Dubey, 1997, Dubey *et al.*, 1997, Barragan and Sibley, 2002), vascular endothelium (Lambert *et al.*, 2006, Furtado *et al.*, 2012), the blood-brain barrier (Courret *et al.*, 2006, Lachenmaier *et al.*, 2011), the retina (Furtado *et al.*, 2013), and the maternal-fetal interface (Robbins *et al.*, 2012).

Research has demonstrated roles for different types of motile immune cells, including monocytes and dendritic cells (DCs), as "Trojan horses" for *T. gondii* dissemination in the host (Tardieux and Menard, 2008). Given the distinct functions and distribution of these immune cell populations, it is likely that they facilitate parasite dissemination in different locations in the body. DCs are predominantly found in tissues and upon activation traffic to lymph nodes, where they serve as antigen-presenting cells to T cells. *T. gondii* infection of DCs induces a hypermigratory phenotype and enhances parasite spread (Lambert *et al.*, 2006). This phenotype is associated with rapid cytoskeletal rearrangement and DC migration (Weidner *et al.*, 2013) and indicates that parasites may disseminate through tissues or to lymph nodes inside DCs (Bierly *et al.*, 2008). In contrast, monocytes are the major immune cell infected by *T. gondii* in peripheral blood (Channon *et al.*, 2000), where DCs are present in very low numbers. Since the primary function of monocytes is to migrate from the bloodstream into tissues (Serbina *et al.*, 2008), they may serve as an ideal vessel for parasite spread from the vasculature into organs. Indeed, infected $CD11b^{+}/CD11c^{-}$ monocytes in the blood have been shown to shuttle parasites to the brain (Courret *et al.*, 2006), and infected $CD11b^{+}/CD11c^{-}$ primary human monocytes migrate more frequently through a blood-brain barrier model than infected $CD11c^{+}$ DC (Lachenmaier *et al.*, 2011).

Blood vessels in the body are lined with endothelial cells that form an effective biological barrier. The translocation of *T. gondii* across endothelium in infected human leukocytes has been clearly demonstrated using transwell assays in static conditions (Lambert *et al.*, 2006, Lachenmaier *et al.*, 2011, Furtado *et al.*, 2012). These assays have contributed important insight into mechanisms of *T. gondii* dissemination; however, static transwell assays are not optimal for visualizing and analyzing early, dynamic events in transmigration (i.e., within minutes of contact with the endothelial barrier), and they do not incorporate the conditions of shear stress found in rapidly flowing blood. In the blood, monocytes tether, roll, and firmly adhere to vascular endothelium using a multi-step cascade that involves well described receptor-ligand interactions, many of which are enhanced due to shear force (Ley *et al.*, 2007). Integrins, heterodimeric adhesion molecules on the monocyte surface, play a central role in extravasation by facilitating firm adhesion to endothelium and subsequent searching/crawling to sites of transendothelial migration (TEM) (Herter and Zarbock, 2013). Disrupting the ability of integrins to interact with ligands on endothelium significantly inhibits TEM (Schenkel *et al.*, 2004). However, the dynamics of infected monocyte TEM, and the molecular mechanisms that facilitate this process are not well understood.

We previously reported the use of a fluidic system to investigate the early events in monocyte interactions with vascular endothelium. Our studies showed that *T. gondii* infection alters the adhesion dynamics of human primary monocytes and THP-1 cells in shear stress conditions and delays the ligand-dependent clustering of the monocyte integrins

LFA-1 (CD11a/CD18) and VLA-4 (CD49d/CD29) (Harker *et al.*, 2013). In the current study, we have examined the step downstream of firm adhesion and specifically investigated the transmigration of infected monocytes across endothelium in static and shear flow conditions. To do so, we adapted our live-cell imaging system to visualize infected monocytes for up to 60 minutes (min) after contact with the endothelium. Analyzing over 3000 monocytes revealed several features of how *T. gondii* crosses endothelial barriers: 1) infected monocytes crawled farther and faster on the endothelial surface than uninfected monocytes before undergoing TEM, but completed TEM rapidly (within ~10 min, on average); 2) shear stress conditions significantly increased the frequency of monocyte TEM compared to static assay conditions; 3) Mac-1 blockade inhibited the crawling and TEM of infected monocytes to a greater degree than uninfected monocytes; and 4) ICAM-1 blockade impaired the crawling and TEM of both infected and uninfected monocytes. Our study visualizes the early events in the intracellular transport of *T. gondii* across human endothelium using real-time microscopy in shear flow conditions and characterizes the involvement of specific adhesion receptors and ligands in this process.

Results

T. gondii undergoes transendothelial migration in primary human monocytes

We first established a live-cell imaging protocol under static conditions to visualize *T. gondii*-infected monocytes performing TEM. Freshly isolated human monocytes from peripheral blood were incubated with green fluorescent protein (GFP)-expressing *T. gondii*. The parasites actively invade monocytes, as shown by vacuolar staining for the dense granule protein GRA7 (Fig. S1A). At 1 hour post-infection (hpi), the monocytes had high viability, and 40% of the monocytes in the culture harbored intracellular parasites and were GFP^+ (Fig. S1B). The combination of infected and uninfected cells in the culture allowed us to visualize TEM of both monocyte populations within the same field of view, thereby minimizing bias when quantifying their respective TEM frequencies. The monocyte cultures were added to chamber slide wells coated with HUVEC monolayers that had been pre-treated with TNF-α and MCP-1 (Carman and Springer, 2004).

In order to verify the endothelial barrier strength of the of the HUVEC monolayer, we performed electric cell-substrate impedance sensing (ECIS) assays. Following our seeding protocol, HUVEC attained visual confluence within 4 hours (h). Transendothelial electrical resistance (TEER) increased rapidly within the first 6 h after seeding and then increased more gradually from 6 h to 24 h (Fig. S1C). These findings are consistent with previous reports showing that HUVEC reach close to maximal TEER values shortly after attaining visual confluence (Dewi *et al.*, 2004, Kluger *et al.*, 2013). The addition of TNF-α and MCP-1 at 25 h post-seeding resulted in a slight increase in capacitance, a measure of permeability, and TEER values indicative of 82.4% of maximal barrier integrity at the time point when TEM assays were performed (4 h post-treatment).

Searching or crawling is defined as monocyte migration on the surface of the endothelium (parallel to the endothelium), whereas TEM is defined as migration through the endothelial barrier (perpendicular to the endothelial cells). Upon contact with the endothelium, uninfected monocytes actively searched/crawled, extending and retracting lamellipodia.

When their leading edge detected what appeared to be an intercellular junction, uninfected monocytes underwent TEM and then regained motility beneath the monolayer. TEM was characterized by a marked change in differential interference contrast (DIC) illumination of the monocyte from bright to dim. At the site of TEM, monocytes stopped crawling and funneled through a narrow portal on the endothelium, a process that appeared to pinch and slightly elongate the cell body and decrease the contrast of light and dark shadows by DIC imaging (Fig. 1A and Video S1). Monocytes infected with *T. gondii* also crawled dynamically, forming cytoplasmic projections to sense the endothelium, and completed TEM (Fig. 1B and Video S2). Notably, the parasites remained intracellular during both monocyte crawling and TEM, and did not egress during the time periods analyzed, up to 60 min post-contact with HUVEC.

Infection alters the dynamics of monocyte crawling and transmigration

We next tracked the monocytes imaged by live-cell microscopy to quantify the dynamics of crawling. When cell movement was tracked during the initial 5 min after contact with the endothelium, *T. gondii*-infected monocytes crawled farther from the point of origin compared to uninfected monocytes (Fig. 2A). During this time, the maximum displacement from the origin was 1.4-fold greater for infected monocytes than uninfected monocytes (Fig. 2B). To further characterize crawling, we quantified the total pathlength (accumulated distance crawled by the cell) and the average velocity of each cell during the 5 min period, as well as the duration of the entire crawling process. Infection increased both the total pathlength and average velocity of monocytes by 1.3-fold (Fig. 2C). On average, uninfected monocytes crawled for 6.5 min before commencing TEM versus 11.1 min for infected monocytes (Fig. 2D).

To quantify monocyte TEM, we determined the TEM frequency from 991 total monocytes that appeared in our fields of view and also calculated the frequency of monocyte TEM at different times following contact with the endothelium. Interestingly, most monocytes completed TEM within minutes, and continued to transmigrate until 40 min post-HUVEC contact. Overall, the TEM frequencies for uninfected and infected monocytes were not significantly different (Fig. 2E). Although uninfected monocytes were more likely to perform TEM during the 0 to 10 min period, infected monocytes transmigrated at later time points, likely due to an increased time spent crawling (Fig. 2D and 2E). Infected monocytes spent more time undergoing TEM than uninfected monocytes (9.8 min versus 4.1 min, respectively) (Fig. 2F). However, there was no correlation between the time spent crawling and the time spent undergoing TEM for either uninfected or infected monocytes (Fig. 2G). These data indicate that compared to uninfected monocytes, infected monocytes crawled farther and at higher velocities on endothelium and required more time to complete TEM, but were comparable in overall TEM frequency.

Intracellular T. gondii localize to the uropod during monocyte transmigration

To further characterize monocyte TEM, we investigated the effect of infection on cell morphology. Uninfected and infected monocytes, which were on average 13.6 μm and 14.3 μm in diameter, respectively, elongated to 20.5 μm and 24.1 μm, respectively, as they performed TEM (Fig. 3A). Although the change in cell length did not differ significantly

between uninfected and infected monocytes (Fig. 3B), TEM of infected monocytes was marked by intracellular tachyzoites localizing to the monocyte uropod in 82.6% of cases (Fig. 1B, 3C, and 3E). When this occurred, the parasite appeared to become lodged at the endothelial junction, anchoring the uropod, and was the final portion of the monocyte to transmigrate (Fig. 3C). In less than 20% of infected monocyte TEM events, tachyzoites remained in the main cell body (Fig. 3D and 3E). Infected monocytes in which the intracellular tachyzoite re-localized to the uropod required more time to complete TEM (11.0 min) than those with tachyzoites in the main cell body (4.6 min), which were more comparable to uninfected monocytes (Fig. 2F and 3F). The duration of TEM was not influenced by the number of intracellular parasites, and most monocytes contained only one parasite during the time period of analysis (Fig. 3G).

Taken together, these data reveal that infected monocytes translocate *T. gondii* across endothelial barriers within minutes, and the parasites remained intracellular and predominantly localized to the uropod during TEM.

Infected monocytes express higher levels of the high-affinity conformation of the integrin Mac-1 (CD11b/CD18)

To identify the molecular mechanisms that may contribute to the differences in crawling and TEM by uninfected and *T. gondii*-infected monocytes, we examined the major monocyte surface integrins. As we previously reported for the THP-1 monocytic cell line (Harker *et al.*, 2013), infection did not alter the total expression of the integrins LFA-1, VLA-4, or Mac-1 on primary human monocytes (Fig. 4A). However, compared to THP-1 cells, primary monocytes expressed over 10-fold higher levels of Mac-1 (Fig. S2A). Among *T. gondii*-infected (GFP^+) monocytes, 98.3% of the cells were Mac-1^{high} (63.9% of the total culture) whereas only 1.7% were Mac-1^{low} (1.1% of the total culture) (Fig. 4A).

Mac-1 binding to the ligand ICAM-1 is dependent on conformational changes that expose the active epitope (Oxvig *et al.*, 1999). Since *in vivo* evidence supports that Mac-1 is involved in monocyte intralumenal crawling (Sumagin *et al.*, 2010), we examined the expression of integrins in their active, high-affinity states using conformation-specific monoclonal antibodies (mAb). The active α_M subunit of Mac-1 (CD11b) was expressed in 78.7% of primary monocytes. Interestingly, 89.6% of infected cells were active α_M^{high} (56% of the total culture), whereas only 10.4% were active α_M^{low} (6.5% of the total culture) (Fig. 4A). Over multiple experiments, the mean fluorescence intensity (MFI) of the active α_M subunit expressed on infected primary monocytes was 1.7-fold higher than the levels on uninfected monocytes, and this difference increased to 2.2-fold when the integrins were stimulated with Mn^{2+} (Fig. 4B). Infected monocytes expressed slightly lower levels of the active β_1 VLA-4 subunit (CD29), but this difference was lost with Mn^{2+} treatment, indicating that infection did not impair the ability of VLA-4 to become activated with divalent cation stimulus.

As noted above, unlike primary monocytes, THP-1 cells express very low levels of both total surface Mac-1 and the active α_M subunit (Fig. S2A). Low expression levels of Mac-1 correlated with reduced crawling distance (Fig. S2B) and the complete absence of TEM for both uninfected and *T. gondii*-infected THP-1 cells. Infection did enhance THP-1 cell

crawling, although the increases in crawling distance and velocity were much smaller compared with those observed for primary monocytes (Fig. S2C). These data indicate that Mac-1 levels on monocytes positively correlate with both crawling distance and TEM frequency.

In addition to expressing integrins in the high-affinity conformation, leukocytes redistribute surface integrins to ligands on the endothelium to facilitate firm adhesion and subsequent TEM (Shaw *et al.*, 2004). To visualize the localization of Mac-1 on infected monocytes during TEM, we used confocal microscopy. Using an experimental set-up similar to the live cell imaging experiments, monocytes infected with GFP-expressing *T. gondii* were added to HUVEC monolayers. Samples were then fixed to catch monocytes in the process of undergoing TEM. The cells were stained for Mac-1 on the monocytes and VE-cadherin on the HUVEC to delineate the intercellular junctions of the endothelial cells. Infected monocytes undergoing TEM were found predominantly near HUVEC junctions, and Mac-1 on these monocytes co-localized with VE-cadherin on the endothelium (Fig. 4C). Orthogonal cross-sections generated from this z-stack showed a monocyte mid-way through transmigration. Most of the monocyte cell body was below the endothelium; however, the parasite remained above the plane of the HUVEC, and Mac-1 surrounded the parasite. This observation is in agreement with our time-lapse movies, which show that the intracellular tachyzoite is most frequently the last part of the monocyte to transmigrate (Fig. 3E, Video S2).

These data demonstrate that *T. gondii*-infected primary monocytes expressed high levels of cell surface Mac-1, which accumulated near endothelial junctions during transmigration, and significantly higher levels of the active, high-affinity conformation of Mac-1 than uninfected monocytes, suggesting a role for Mac-1 in both crawling and TEM by *T. gondii*-infected monocytes.

Crawling and transmigration of infected monocytes are mediated by Mac-1 under conditions of fluidic shear stress

We next determined the role of Mac-1 in infected monocyte crawling by performing function-blocking assays. Under conditions of physiologic shear stress, integrin affinity for ligand is up-regulated by “inside-out” selectin- and chemokine-mediated activation, leading to structural changes in the integrin that result in high affinity binding to ligand (Kinashi, 2005). To investigate the role of Mac-1 in the crawling and TEM of *T. gondii*-infected monocytes under these conditions, we used our fluidic and time-lapse imaging system (Harker *et al.*, 2013) and the anti-Mac-1 mAb M1/70, which neutralizes CD11b function *in vitro* (Fan and Edgington, 1993) and *in vivo* (Leon *et al.*, 2006, Auffray *et al.*, 2007). Confluent monolayers of HUVEC in fluidic channels were treated with TNF-α and MCP-1. Monocytes were infected with *T. gondii*, and the culture was treated with anti-Mac-1 mAb or control IgG and flowed through the channels at a shear stress of 0.5 dyn/cm^2. This level of shear stress induces selectin-mediated leukocyte rolling (Lawrence *et al.*, 1997) and is consistent with shear forces found in the bloodstream (Papaioannou and Stefanadis, 2005). For control IgG-treated monocytes, infection increased the total pathlength and average velocity during crawling by 1.4-fold (Fig. 5A-C). The extended crawling of infected

monocytes was inhibited by Mac-1 blockade, which diminished the total pathlength and average velocity of infected monocytes by 1.3-fold (Fig. 5A-C, Video S3 and S4). In contrast, crawling of uninfected monocytes was not significantly affected by Mac-1 blockade in either shear stress (Fig. 5B and 5C) or static conditions (Fig. S3A), indicating that infected cells preferentially use Mac-1 for long-distance crawling.

Remarkably, 45.2% of control IgG-treated infected monocytes performed TEM in shear stress conditions (Fig. 5D), a notable increase compared to the TEM frequencies in static culture (Fig. 2E and S3B). Overall, there was no significant difference between the TEM frequencies of control IgG-treated uninfected and infected monocytes. Mac-1 blockade had the most striking impact on infected monocyte TEM within 10 min post-contact with HUVEC: anti-Mac-1 treatment decreased the cumulative TEM frequency for infected monocytes from 45.2% to 28.1%, whereas the reduction in TEM frequency for uninfected monocytes was from 61.9% to 51.3% (Fig. 5D). We therefore conclude that under conditions of shear stress, the Mac-1 integrin plays a greater role in the crawling and TEM of infected monocytes than uninfected monocytes.

ICAM-1 contributes to uninfected and infected monocyte crawling and transmigration

Lastly, to confirm the significance of Mac-1 function in *T. gondii*-infected monocyte crawling and TEM, we blocked the natural ligand on the endothelium, ICAM-1, using a neutralizing mAb, clone HCD54 (Formoso *et al.*, 2011). In these experiments, the HUVEC monolayer in the fluidic channel was pre-treated with TNF-α, MCP-1, and either anti-ICAM-1 mAb or control IgG. Monocytes were then flowed through at a shear stress of 0.5 dyn/cm^2. Infected monocytes exhibited enhanced crawling on control IgG-treated endothelium (Fig 6A and Video S5), which decreased with ICAM-1 blockade (Fig. 6A, 6B, and Video S6). Both the crawling pathlength and velocity of infected monocytes was reduced by over 1.8-fold due to ICAM-1 blockade, a reduction that exceeded that of uninfected monocytes (1.4-fold; Fig. 6C).

Similar to what was observed in monocytes incubated with control IgG (in Fig. 5D), 42.1% of *T. gondii*-infected monocytes underwent TEM across control IgG-treated endothelium, and the cumulative TEM frequency between uninfected and infected monocytes was not statistically different (Fig. 6D). Compared to control IgG treatment, ICAM-1 blockade disrupted TEM for both uninfected and infected monocytes, decreasing TEM frequency by 2.8-fold and 2.3-fold, respectively (Fig. 6D). We conclude from these experiments that engaging ICAM-1 on the endothelium contributes significantly to TEM for uninfected and infected monocytes.

Discussion

There is strong evidence for a role of immune cells in *T. gondii* dissemination, and transwell systems have convincingly demonstrated the potential of a leukocyte “Trojan horse.” In these previous studies, TEM was measured after several hours of incubation in static culture, ranging from 3 h to 18 h, and the authors documented that a greater number of *T. gondii*-infected murine monocytes (Lachenmaier *et al.*, 2011), murine DC (Lambert *et al.*, 2006), or human DC (Furtado *et al.*, 2012) transmigrated than uninfected cells. We have used a live-

cell imaging approach to examine the first hour after infected human monocytes contact endothelium in static and fluidic shear stress conditions. Our system revealed key differences between how infected and uninfected monocytes interact with the endothelium, and that despite appreciable changes in crawling and TEM dynamics, infected monocytes crossed endothelial barriers within minutes, with intracellular parasites intact (Fig. 7).

Strikingly, in shear stress conditions over 40% of infected monocytes transmigrated within 30 min, a frequency that far exceeded those from previously published static transwell experiments (Lambert *et al.*, 2006, Lachenmaier *et al.*, 2011, Furtado *et al.*, 2012) and from our own static assay conditions (Fig. 2). This finding reinforces that shear forces considerably affect the molecular interactions between monocytes and endothelial cells. Monocyte tethering to the endothelial surface is mediated by selectin-selectin ligand interactions that lead to rolling, during which monocyte chemokine receptors scan for chemokines displayed on the endothelium (Ley *et al.*, 2007). The signaling events from these dynamic interactions enhance the function of monocyte integrins (Zarbock *et al.*, 2011), which likely contributes to the increased speed and frequency of TEM in conditions of shear stress. Activation of HUVEC with TNF-α and MCP-1 (Lachenmaier *et al.*, 2011), which mimics *T. gondii*-induced systemic inflammation (Aviles *et al.*, 2008), is also known to enhance monocyte migration in response to infection (Robben *et al.*, 2005).

In orally-infected mice, monocytes encounter *T. gondii* in the lamina propria (Coombes *et al.*, 2013, Gregg *et al.*, 2013), and $CD11b^{+}CD11c^{-}$ monocytes have been shown to be the predominant blood leukocyte population to shuttle parasites to the brain (Courret *et al.*, 2006). Parasites administered intravenously are detectable in organs as early as 2 h post-tail vein injection (Unno *et al.*, 2013). These data, in conjunction with our current findings suggest that monocytes may traffic *T. gondii* across endothelial barriers and into tissues very rapidly after infection. The degree of temporal detail obtained from real-time microscopy is highly informative for dissecting the dynamics and the molecular mechanisms of infected monocyte crawling and TEM. We have observed that the transmigration of infected monocytes required more time than that of uninfected monocytes. This may be due, in part, to the rigid cytoskeleton of the parasite, which appeared to become temporarily lodged at the endothelial barrier. This process likely imparts a physical force on the endothelium as well as on the amoeboid monocyte undergoing TEM. Remarkably, despite the constraint imposed by the intracellular parasite, we never observed parasite egress or monocyte lysis during TEM. We did observe extracellular parasites in the culture adhering to HUVEC in conditions of shear stress. Since tachyzoites are highly motile and can transmigrate across cellular barriers (Barragan *et al.*, 2005), this suggests that TEM by extracellular parasites may serve as an additional mode of dissemination from the vasculature.

Integrin expression is tightly linked to cytoskeletal rearrangement and consequently cell motility (Nayal *et al.*, 2004). We previously reported that *T. gondii*-infected THP-1 cells are impaired in LFA-1 and VLA-4 integrin clustering to ligands and in pseudopod extension (Harker *et al.*, 2013). In concert with these observations, it was recently shown that *T. gondii*-infected human DCs exhibit profound changes in the DC cytoskeleton, which is linked to a decrease in surface CD18 redistribution and an increase in CCR7 expression (Weidner *et al.*, 2013). It is possible that integrin dysregulation is an active process by the

parasite for altering the dynamics of leukocyte movement (Da Gama *et al.*, 2004). In infected DCs, *T. gondii* dense granule protein GRA5 induces CCR7-mediated chemotaxis (Persat *et al.*, 2012). In murine macrophages, *T. gondii* infection induces an increase in the expression of ADAM10 (Seipel *et al.*, 2010), a transmembrane metalloproteinase. Notably, ADAM10 and the related ADAM17 metalloproteinase cleave Mac-1 to regulate monocyte diapedesis, and ADAM17 activity facilitates human monocyte transmigration through HUVEC (Tsubota *et al.*, 2013). We observed that ~90% of *T. gondii*-infected monocytes expressed the active conformation of the Mac-1 α_M subunit (CD11b), and Mac-1 played a key role in *T. gondii*-infected monocyte crawling and TEM. Whether parasite infection alters Mac-1 activity or *T. gondii* preferentially infects a subset of active Mac-1^{high} human monocytes is currently under investigation.

Monocyte crawling and extravasation are orchestrated by the overlapping functions of Mac-1 and LFA-1 (Herter and Zarbock, 2013), and intravital microscopy revealed that Mac-1-mediated crawling is enhanced in monocytes during inflammation (Sumagin *et al.*, 2010). Following *T. gondii* infection of human monocytes, we found that the levels of active Mac-1 increased, and both crawling and TEM were inhibited by neutralizing Mac-1 or its ligand ICAM-1. ICAM-1 recognizes both Mac-1 and LFA-1, and HUVEC treated with anti-ICAM-1 mAb that blocks binding to Mac-1, but not LFA-1, still interact extensively with monocytes (Carman *et al.*, 2003). Our findings may be indicative of such shared roles of these monocyte integrins on infected cells. Although we did not detect an increase in Mac-1 expression or activation when monocytes were subject to fluidic shear stress (Fig. S4), the Mac-1-ICAM-1 interaction may nevertheless predominate during *T. gondii* infection (Courret *et al.*, 2006, Furtado *et al.*, 2012). In addition to chemokine- and selectin-mediated “inside-out” activation, Mac-1 binding affinity is also increased by “outside-in” activation (Lim and Hotchin, 2012), which results in integrin re-localization and clustering to ligands on the endothelium (Abram and Lowell, 2009). Indeed, TEM of *T. gondii*-infected monocytes was marked by co-localization of monocyte Mac-1 with VE-cadherin on HUVEC, suggesting that the integrin detects proteins near endothelial junctions and that they facilitate TEM at or near this site.

This research delineates a pathway for the translocation of intracellular *T. gondii* across endothelium and characterizes the effects of infection on monocyte transmigration. Furthermore, these findings contribute to an understanding of integrin function in the context of infection and mechanisms that differentially mediate the migration of infected and uninfected cells. This information may lay the groundwork for future efforts to identify potential targets for combating pathogen spread and disease in the infected host without impairing the protective immune function of monocytes during infection.

Experimental procedures

Mammalian and parasite cell culture

Human peripheral blood was generously provided by the Healthy Donor Program of the Institute for Clinical and Translational Science (ICTS) at the University of California, Irvine and was used to harvest mononuclear cells, with approval from the Institutional Review Board. Primary human monocytes were isolated by counter-flow elutriation using a

modification of the technique of Lionetti et al. (Lionetti *et al.*, 1980), as previously described (Bobak *et al.*, 1986). Isolated monocytes were used immediately for experimentation. THP-1 cells were cultured in RPMI 1640 (Hyclone, Logan, UT) supplemented with 10% heat-inactivated FBS (Omega Scientific, Tarzana, CA), 2 mM L-glutamine, 100 U/ml penicillin, and 100 μg/ml streptomycin (R-10 medium). HUVEC were cultured in EGM-2 medium plus EGM-2 SingleQuot supplements and growth factors (Lonza, Allendal, NJ). Type II *T. gondii* (*Prugniaud*) tachyzoites expressing GFP were maintained in human foreskin fibroblasts (HFF) and were syringe-lysed and washed immediately before experimentation, as previously described (Morgado *et al.*, 2011). With the exception of the experiments using THP-1 cells in Supplemental Figure S2, primary human monocytes were used in all assays. Parasites were added to monocytes or THP-1 cells at a MOI (multiplicity of infection) of 2.5. Infections were performed for 1 h in R-10 medium. Uninfected cells were cultured in parallel. All parasite and human cell cultures were tested monthly for *Mycoplasma* contamination and confirmed to be negative.

HUVEC barrier formation and transendothelial electrical resistance assays

Assays in static conditions were performed using a modified protocol previously described for imaging monocyte TEM (Carman and Springer, 2004): wells on 8-well chamber slides (Thermo Scientific, Rockford, IL) or coverslips in 24-well tissue culture plates were coated with 1% gelatin and 20 μg/ml fibronectin and seeded with 6×10^4 or 1.5×10^5 HUVEC, respectively. After 4 h, HUVEC were confirmed to be confluent by microscopy and were then cultured for an additional 21 h. Assays under fluidic shear stress were performed using fluidic devices that were fabricated as previously described (Harker *et al.*, 2013). Devices were coated with 1% gelatin and 20 μg/ml fibronectin and seeded with 2.5×10^5 HUVEC. Before each experiment, the monolayer was activated with 20 ng/ml TNF-α and 200 ng/ml MCP-1 for 4 h.

To test the barrier integrity of HUVEC following our seeding protocol, ECIS assays were used. Briefly, a 96-well electrode array (20 interdigitated electrode fingers with a total area of 3.92 mm^2, Applied Biophysics, Troy, NY) was coated with 1% gelatin and 20 μg/ml fibronectin, and 5×10^4 HUVEC were seeded into each well. Immediately after seeding, the array was placed on an ECIS Zθ (Applied Biophysics), maintained at 37°C and 5% CO_2, and the impedance was measured every 30 min at multiple AC frequencies. At 25 h, 20 ng/ml TNF-α and 200 ng/ml MCP-1 were added to the test wells, and the assay was carried out for an additional 23 h. Impedance measured at 4000 Hz and 64000 Hz were used to calculate resistance and capacitance, respectively. Resistance was then multiplied by the surface area of the ECIS electrodes to calculate TEER values (Benson *et al.*, 2013).

Transendothelial migration assays

For assays in static conditions, 1.5×10^5 uninfected and *T. gondii*-infected monocytes or THP-1 cells were added per well on 8-well chamber slides. After a well was inoculated, the slide was mounted on the stage, the microscope was focused to the top surface of the endothelium, and imaging was immediately initiated. Time-lapse DIC and fluorescence images (for GFP) were acquired every 10 seconds for up to 1 h using a 10X or 20X objective, and the slide was maintained at 37°C and 5% CO_2 in a UNO environmental

chamber (OkoLab, Ottaviano, NA, Italy). A Nikon Eclipse Ti inverted fluorescent microscope with NIS-Elements acquisition software (Nikon Instruments, Melville, NY) was used for imaging.

For assays under shear stress, 1×10^7 uninfected and *T. gondii*-infected monocytes were flowed through fluidic channels. Fluidic shear stress was maintained at 0.5 dyn/cm^2 using a Model '11' Plus dual syringe pump (Harvard Apparatus, Holliston, MA). After the monocytes were flowed into the device for 5 to 10 min, a y-valve connector was used to immediately perfuse RPMI 1640 media through the device without disrupting flow for an additional 30 min at the same flow rate. Fluidic devices were maintained in the environmental chamber for the duration of the time-lapse microscopy. For measuring integrin expression levels under shear stress, monocytes were collected on ice into reservoirs connected to the exit ports of the fluidic devices and immediately processed for flow cytometry.

For Mac-1 neutralization assays, monocytes were resuspended at 2×10^6/ml and treated with 10 μg/ml anti-Mac-1 mAb (M1/70, Bio X Cell, West Lebanon, NH) or rat control IgG2b (RTK4530, Biolegend, San Diego, CA) for 15 min at 37°C. Untreated monocytes were incubated in parallel. Following antibody treatment, monocytes were immediately added to the chamber slide wells or fluidic devices. For ICAM-1 neutralization assays, HUVEC monolayers in fluidic devices were treated with 20 μg/ml anti-ICAM-1 (HCD54, Biolegend) or mouse control IgG1 (P3, eBioscience, San Diego, CA) for 15 min at 37°C. Monocytes were then flowed into the fluidic devices as described.

Cell tracking and analysis

Monocytes were tracked using the time-lapse DIC and fluorescent images generated from the TEM assays. Monocytes containing at least one GFP$^+$ *T. gondii* tachyzoite were counted as infected. The length of time spent crawling was defined as the time spent moving parallel to the endothelium, from the moment of monocyte contact with the endothelium to the start of TEM. During crawling, monocytes appeared spherical and bright under DIC illumination. The length of time spent transmigrating was defined as the time spent moving perpendicular to and through the endothelium, from the start of TEM to the end of TEM when the monocytes had dimmed under DIC illumination.

For calculating changes in cell length, the distance between the leading edge and the uropod was measured when the monocyte first entered the plane of focus and contacted HUVEC, and again when the monocyte became most elongated during TEM. Only monocytes that completed TEM were analyzed for cell length, crawling time and transmigration time. For analyzing crawling, the position and the instantaneous velocity of individual monocytes were recorded by tracking the center of the cells in each frame. Crawling was tracked for 5 min (30 frames) from the time of contact with the HUVEC, since uninfected monocytes started TEM after crawling on average for 6.7 min. These data were used to calculate the total pathlength, maximum displacement, and average velocity of each cell. For the motility "flower" plots, the position of the monocyte when it first contacted the endothelium was placed at the origin (0, 0). The x- and y-coordinates in the subsequent frames were then used

to plot monocyte location during crawling for 5 min. For these analyses, the monocytes were chosen at random and were not required to have completed TEM.

ImageJ software with the Manual Tracking plugin was used for all cell tracking and analysis. Prism (GraphPad Software, La Jolla, CA) was used to graph the tracking data.

Flow cytometry

Uninfected monocytes and *T. gondii*-infected monocytes at 1 hpi were treated with 7-AAD viability dye (Biolegend) to determine the infection efficiency and the viability of the monocyte cultures. Integrin expression and activation were determined as previously described (Harker *et al.*, 2013). The following mAb against total and active conformation integrins were used: LFA-1/α_L (TS2/4), VLA-4/α_4 (9F10), or Mac-1/α_M (ICRF44), or active β_2 integrin (24), active β_1 integrin (12G10), or active α_M integrin (CBRM1/5, PE-conjugated). Mouse IgG1κ (P3) or PE-conjugated IgG1 κ (MOPC-21) were used for controls. All antibodies were obtained from BioLegend, except for clones 24 and 12G10 (Abcam, Cambridge, MA). BD FACSCalibur, CellQuest Pro software (BD Biosciences, San Jose, CA), and FlowJo software (Tree Star, Ashland, OR) were used for analysis.

Immunofluorescence microscopy

To visualize parasite invasion of monocytes, 2.5×10^5 uninfected and *T. gondii*-infected monocytes at approximately a 1:1 ratio were settled onto fibronectin-coated coverslips for 5 min at 37°C. Samples were fixed, permeabilized, and stained for vacuolar GRA7 as previously described (Dunn *et al.*, 2008). Anti-GRA7 antibody (12B6) was a generous gift from P. Bradley (University of California, Los Angeles). To visualize monocyte TEM, 2.5×10^5 uninfected and *T. gondii*-infected monocytes at approximately a 1:1 ratio were settled onto HUVEC-coated coverslips for 1 h at 37°C. Samples were fixed with 4% PFA (Electron Microscopy Sciences, Hatfield, PA), blocked with PBS containing 5% NGS (Life Technologies, Carlsbad, CA) and 1% BSA, and stained with anti-Mac-1/α_M (M1/70) and anti-VE-cadherin (BV9) mAbs (Biolegend). Alexa Fluor 594-conjugated goat anti-rat IgG and Alexa Fluor 350-conjugated goat anti-mouse IgG (Life Technologies) were used as secondary antibodies. Coverslips were mounted using VectaShield with DAPI (Vector Laboratories, Burlingame, CA). Confocal microscopy was performed using a Nikon Eclipse Ti inverted microscope with a 60X objective, as previously described (Harker *et al.*, 2013).

For quantifying the frequency of TEM, 0.5 μm confocal z-sections were imaged using a 40X objective. The percent of monocytes that were entirely or partially below the endothelial plane (defined by VE-cadherin staining of intercellular junctions) was calculated relative to total adhered monocytes, and the results were plotted using Prism software.

Statistics

Statistical analysis was performed using Prism software. Linear regression was calculated from the best fit slope in Figs. 2B, 2G, 5B, and 6B. The Student's *t*-test with Welch's correction was used for pairwise comparisons in Figs. 2C-F, 3A, 3B, 3E, 3F, 4B, 5C, 5D, 6C, 6D, S2C, S3A, and S3B. One way ANOVA with a Tukey comparison was used to compare all means in Fig. 3G.

Supplementary Material

Refer to Web version on PubMed Central for supplementary material.

Acknowledgments

This work was supported by ACS IRG-98-279-07 (M.B.L.), AHA Scientist Development Grant 10SDG3140025 (M.B.L.), AHA Postdoctoral Fellowship 13POST14580034 (N.U.), and set-up funds from the UC Irvine School of Biological Sciences (M.B.L.). NIH Immunology Training Grant T32AI60573 (K.S.H.), NIH A141090 (A.T. and E.V.C.), NIH NIDCR DP2DE023319 (W.F.L), NIH T32 Systems Biology of Development Training Grant (F.Y.M.). We thank all members of the Tenner, Nelson, Prescher, and Morrissette labs for helpful discussion on this project. We also thank Dr. Michael Buchmeier for the generous use of the Nikon Eclipse Ti microscope, Dr. Dritan Agalliu and Dr. Sarah Lutz for the generous use of the ECIS Zθ instrument and for their expertise on endothelial barrier integrity, and the UC Irvine ICTS for providing healthy donor blood for monocyte isolations.

References

Abram CL, Lowell CA. The ins and outs of leukocyte integrin signaling. Annu Rev Immunol. 2009; 27:339–362. [PubMed: 19302044]

Auffray C, Fogg D, Garfa M, Elain G, Join-Lambert O, Kayal S, et al. Monitoring of blood vessels and tissues by a population of monocytes with patrolling behavior. Science. 2007; 317:666–670. [PubMed: 17673663]

Aviles H, Stiles J, O'Donnell P, Orshal J, Leid J, Sonnenfeld G, Monroy F. Kinetics of systemic cytokine and brain chemokine gene expression in murine toxoplasma infection. J Parasitol. 2008; 94:1282–1288. [PubMed: 19127964]

Barragan A, Brossier F, Sibley LD. Transepithelial migration of Toxoplasma gondii involves an interaction of intercellular adhesion molecule 1 (ICAM-1) with the parasite adhesin MIC2. Cell Microbiol. 2005; 7:561–568. [PubMed: 15760456]

Barragan A, Sibley LD. Transepithelial migration of Toxoplasma gondii is linked to parasite motility and virulence. J Exp Med. 2002; 195:1625–1633. [PubMed: 12070289]

Barragan A, Sibley LD. Migration of Toxoplasma gondii across biological barriers. Trends Microbiol. 2003; 11:426–430. [PubMed: 13678858]

Benson K, Cramer S, Galla HJ. Impedance-based cell monitoring: barrier properties and beyond. Fluids Barriers CNS. 2013; 10:5. [PubMed: 23305242]

Bierly AL, Shufesky WJ, Sukhumavasi W, Morelli AE, Denkers EY. Dendritic cells expressing plasmacytoid marker PDCA-1 are Trojan horses during Toxoplasma gondii infection. J Immunol. 2008; 181:8485–8491. [PubMed: 19050266]

Bobak DA, Frank MM, Tenner AJ. Characterization of C1q receptor expression on human phagocytic cells: effects of PDBu and fMLP. J Immunol. 1986; 136:4604–4610. [PubMed: 3486907]

Carman CV, Jun CD, Salas A, Springer TA. Endothelial cells proactively form microvilli-like membrane projections upon intercellular adhesion molecule 1 engagement of leukocyte LFA-1. J Immunol. 2003; 171:6135–6144. [PubMed: 14634129]

Carman CV, Springer TA. A transmigratory cup in leukocyte diapedesis both through individual vascular endothelial cells and between them. J Cell Biol. 2004; 167:377–388. [PubMed: 15504916]

Channon JY, Seguin RM, Kasper LH. Differential infectivity and division of Toxoplasma gondii in human peripheral blood leukocytes. Infect Immun. 2000; 68:4822–4826. [PubMed: 10899898]

Coombes JL, Charsar BA, Han SJ, Halkias J, Chan SW, Koshy AA, et al. Motile invaded neutrophils in the small intestine of Toxoplasma gondii-infected mice reveal a potential mechanism for parasite spread. Proc Natl Acad Sci U S A. 2013; 110:E1913–1922. [PubMed: 23650399]

Courret N, Darche S, Sonigo P, Milon G, Buzoni-Gatel D, Tardieux I. CD11c- and CD11b-expressing mouse leukocytes transport single Toxoplasma gondii tachyzoites to the brain. Blood. 2006; 107:309–316. [PubMed: 16051744]

Da Gama LM, Ribeiro-Gomes FL, Guimaraes U Jr. Arnholdt AC. Reduction in adhesiveness to extracellular matrix components, modulation of adhesion molecules and in vivo migration of

murine macrophages infected with Toxoplasma gondii. Microbes Infect. 2004; 6:1287–1296. [PubMed: 15555535]

Dewi BE, Takasaki T, Kurane I. In vitro assessment of human endothelial cell permeability: effects of inflammatory cytokines and dengue virus infection. J Virol Methods. 2004; 121:171–180. [PubMed: 15381354]

Dubey JP. Bradyzoite-induced murine toxoplasmosis: stage conversion, pathogenesis, and tissue cyst formation in mice fed bradyzoites of different strains of Toxoplasma gondii. J Eukaryot Microbiol. 1997; 44:592–602. [PubMed: 9435131]

Dubey JP, Speer CA, Shen SK, Kwok OC, Blixt JA. Oocyst-induced murine toxoplasmosis: life cycle, pathogenicity, and stage conversion in mice fed Toxoplasma gondii oocysts. J Parasitol. 1997; 83:870–882. [PubMed: 9379292]

Dunn JD, Ravindran S, Kim SK, Boothroyd JC. The Toxoplasma gondii dense granule protein GRA7 is phosphorylated upon invasion and forms an unexpected association with the rhoptry proteins ROP2 and ROP4. Infect Immun. 2008; 76:5853–5861. [PubMed: 18809661]

Fan ST, Edgington TS. Integrin regulation of leukocyte inflammatory functions. CD11b/CD18 enhancement of the tumor necrosis factor-alpha responses of monocytes. J Immunol. 1993; 150:2972–2980. [PubMed: 8095957]

Formoso G, Di Tomo P, Andreozzi F, Succurro E, Di Silvestre S, Prudente S, et al. The TRIB3 R84 variant is associated with increased carotid intima-media thickness in vivo and with enhanced MAPK signalling in human endothelial cells. Cardiovasc Res. 2011; 89:184–192. [PubMed: 20693163]

Furtado JM, Ashander LM, Mohs K, Chipps TJ, Appukuttan B, Smith JR. Toxoplasma gondii migration within and infection of human retina. PLoS One. 2013; 8:e54358. [PubMed: 23437042]

Furtado JM, Bharadwaj AS, Ashander LM, Olivas A, Smith JR. Migration of toxoplasma gondii-infected dendritic cells across human retinal vascular endothelium. Invest Ophthalmol Vis Sci. 2012; 53:6856–6862. [PubMed: 22952125]

Gregg B, Taylor BC, John B, Tait-Wojno ED, Girgis NM, Miller N, et al. Replication and distribution of Toxoplasma gondii in the small intestine after oral infection with tissue cysts. Infect Immun. 2013; 81:1635–1643. [PubMed: 23460516]

Harker KS, Ueno N, Wang T, Bonhomme C, Liu W, Lodoen MB. Toxoplasma gondii modulates the dynamics of human monocyte adhesion to vascular endothelium under fluidic shear stress. J Leukoc Biol. 2013; 93:789–800. [PubMed: 23485448]

Herter J, Zarbock A. Integrin Regulation during Leukocyte Recruitment. J Immunol. 2013; 190:4451–4457. [PubMed: 23606722]

Kinashi T. Intracellular signalling controlling integrin activation in lymphocytes. Nat Rev Immunol. 2005; 5:546–559. [PubMed: 15965491]

Kluger MS, Clark PR, Tellides G, Gerke V, Pober JS. Claudin-5 controls intercellular barriers of human dermal microvascular but not human umbilical vein endothelial cells. Arterioscler Thromb Vasc Biol. 2013; 33:489–500. [PubMed: 23288152]

Lachenmaier SM, Deli MA, Meissner M, Liesenfeld O. Intracellular transport of Toxoplasma gondii through the blood-brain barrier. J Neuroimmunol. 2011; 232:119–130. [PubMed: 21106256]

Lambert H, Hitziger N, Dellacasa I, Svensson M, Barragan A. Induction of dendritic cell migration upon Toxoplasma gondii infection potentiates parasite dissemination. Cell Microbiol. 2006; 8:1611–1623. [PubMed: 16984416]

Lawrence MB, Kansas GS, Kunkel EJ, Ley K. Threshold levels of fluid shear promote leukocyte adhesion through selectins (CD62L,P,E). J Cell Biol. 1997; 136:717–727. [PubMed: 9024700]

Leon F, Contractor N, Fuss I, Marth T, Lahey E, Iwaki S, et al. Antibodies to complement receptor 3 treat established inflammation in murine models of colitis and a novel model of psoriasiform dermatitis. J Immunol. 2006; 177:6974–6982. [PubMed: 17082612]

Ley K, Laudanna C, Cybulsky MI, Nourshargh S. Getting to the site of inflammation: the leukocyte adhesion cascade updated. Nat Rev Immunol. 2007; 7:678–689. [PubMed: 17717539]

Lim J, Hotchin NA. Signalling mechanisms of the leukocyte integrin alphaMbeta2: current and future perspectives. Biol Cell. 2012; 104:631–640. [PubMed: 22804617]

Lionetti, FJ.; Hunt, SM.; Valeri, CR. Isolation of human blood phagocytes by counterflow centrifugation elutriation. In: Catsimpoolas, N., editor. Methods of Cell Separation. Springer US; New York: 1980. p. 141-156.

Montoya JG, Liesenfeld O. Toxoplasmosis. Lancet. 2004; 363:1965–1976. [PubMed: 15194258]

Morgado P, Ong YC, Boothroyd JC, Lodoen MB. Toxoplasma gondii induces B7-2 expression through activation of JNK signal transduction. Infect Immun. 2011; 79:4401–4412. [PubMed: 21911468]

Nayal A, Webb DJ, Horwitz AF. Talin: an emerging focal point of adhesion dynamics. Curr Opin Cell Biol. 2004; 16:94–98. [PubMed: 15037311]

Oxvig C, Lu C, Springer TA. Conformational changes in tertiary structure near the ligand binding site of an integrin I domain. Proc Natl Acad Sci U S A. 1999; 96:2215–2220. [PubMed: 10051621]

Papaioannou TG, Stefanadis C. Vascular Wall Shear Stress: Basic Principles and Methods. Hellenic Journal of Cardiology. 2005; 46:9–15. [PubMed: 15807389]

Persat F, Mercier C, Ficheux D, Colomb E, Trouillet S, Bendridi N, et al. A synthetic peptide derived from the parasite Toxoplasma gondii triggers human dendritic cells' migration. J Leukoc Biol. 2012; 92:1241–1250. [PubMed: 23033174]

Robben PM, LaRegina M, Kuziel WA, Sibley LD. Recruitment of Gr-1+ monocytes is essential for control of acute toxoplasmosis. J Exp Med. 2005; 201:1761–1769. [PubMed: 15928200]

Robbins JR, Zeldovich VB, Poukchanski A, Boothroyd JC, Bakardjiev AI. Tissue barriers of the human placenta to infection with Toxoplasma gondii. Infect Immun. 2012; 80:418–428. [PubMed: 22083708]

Schenkel AR, Mamdouh Z, Muller WA. Locomotion of monocytes on endothelium is a critical step during extravasation. Nat Immunol. 2004; 5:393–400. [PubMed: 15021878]

Seipel D, Oliveira BC, Resende TL, Schuindt SH, Pimentel PM, Kanashiro MM, Arnholdt AC. Toxoplasma gondii infection positively modulates the macrophages migratory molecular complex by increasing matrix metalloproteinases, CD44 and alpha v beta 3 integrin. Vet Parasitol. 2010; 169:312–319. [PubMed: 20080350]

Serbina NV, Jia T, Hohl TM, Pamer EG. Monocyte-mediated defense against microbial pathogens. Annu Rev Immunol. 2008; 26:421–452. [PubMed: 18303997]

Shaw SK, Ma S, Kim MB, Rao RM, Hartman CU, Froio RM, et al. Coordinated redistribution of leukocyte LFA-1 and endothelial cell ICAM-1 accompany neutrophil transmigration. J Exp Med. 2004; 200:1571–1580. [PubMed: 15611287]

Sumagin R, Prizant H, Lomakina E, Waugh RE, Sarelius IH. LFA-1 and Mac-1 define characteristically different intralumenal crawling and emigration patterns for monocytes and neutrophils in situ. J Immunol. 2010; 185:7057–7066. [PubMed: 21037096]

Tardieux I, Menard R. Migration of Apicomplexa across biological barriers: the Toxoplasma and Plasmodium rides. Traffic. 2008; 9:627–635. [PubMed: 18194412]

Tsubota Y, Frey JM, Tai PW, Welikson RE, Raines EW. Monocyte ADAM17 promotes diapedesis during transendothelial migration: identification of steps and substrates targeted by metalloproteinases. J Immunol. 2013; 190:4236–4244. [PubMed: 23479224]

Unno A, Kachi S, Batanova TA, Ohno T, Elhawary N, Kitoh K, Takashima Y. Toxoplasma gondii tachyzoite-infected peripheral blood mononuclear cells are enriched in mouse lungs and liver. Exp Parasitol. 2013; 134:160–164. [PubMed: 23538031]

Weidner JM, Kanatani S, Hernandez-Castaneda MA, Fuks JM, Rethi B, Wallin RP, Barragan A. Rapid cytoskeleton remodelling in dendritic cells following invasion by Toxoplasma gondii coincides with the onset of a hypermigratory phenotype. Cell Microbiol. 2013; 15:1735–1752. [PubMed: 23534541]

Zarbock A, Ley K, McEver RP, Hidalgo A. Leukocyte ligands for endothelial selectins: specialized glycoconjugates that mediate rolling and signaling under flow. Blood. 2011; 118:6743–6751. [PubMed: 22021370]

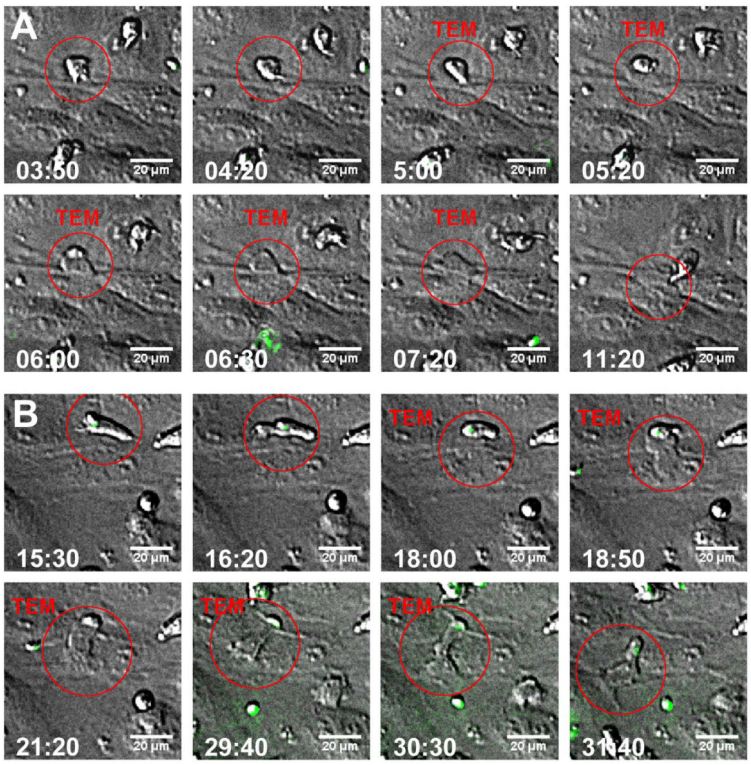

Figure 1.

Transmigration of *T. gondii*-infected monocytes across endothelial monolayers. Monocytes were infected with GFP$^+$ *T. gondii* at a MOI of 2.5 for 1 h and were added to a HUVEC monolayer. (A) Uninfected and (B) *T. gondii*-infected monocytes performing crawling (moving parallel to endothelium) and TEM (moving perpendicular to endothelium) were imaged in real-time using DIC and fluorescence microscopy. Red circles indicate the cell of interest. GFP$^+$ parasites are shown in green. Time-lapse images that show monocyte TEM are marked with “TEM”. Time stamps indicate min:sec after monocyte contact with the endothelium. Representative cells from 7 independent experiments are shown.

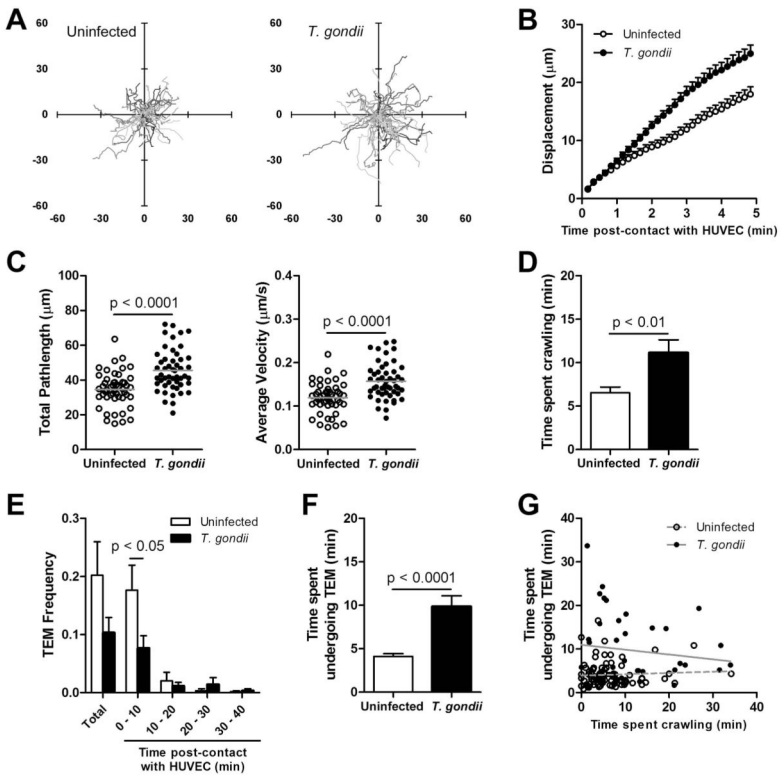

Figure 2.

Crawling and TEM dynamics of uninfected and *T. gondii*-infected monocytes. (A) Motility plots from each monocyte during crawling were generated using cell tracking data from the initial 5 min of crawling. Axes show the distance in μm. (B) Monocyte displacement from the origin during crawling was plotted with respect to time post-contact with endothelium. Data points represent the mean ± SEM. The slopes of the lines are significantly different ($p < 0.0001$). (C) Crawling was quantified by calculating the total pathlength and average velocity of each monocyte for 5 min. Gray lines represent the means. (D) Time spent crawling was quantified by calculating the time from initial contact with the endothelium to the start of TEM. Bars represent the mean ± SEM. (E) TEM frequency was quantified from the total number of monocytes that appeared in the field of view and further characterized based on the time spent crawling by the monocyte prior to TEM. Bars represent the mean ± SEM. (F) Time spent undergoing TEM was quantified by calculating the time from the start of TEM until TEM completion. Bars represent the mean ± SEM. (G) Time spent undergoing TEM was plotted for each monocyte with respect to time spent crawling. Dotted and solid gray lines represent the best fit lines for uninfected and infected monocytes, respectively. For both lines, the slopes are not significantly different from 0. For A-C, $n_{uninfected} = 50$, $n_{T.\ gondii} = 50$ from 4 independent experiments. For D, F, and G, $n_{uninfected} = 83$, $n_{T.\ gondii} = 39$ from 7 independent experiments. For E, $n_{uninfected} = 83$ transmigrated monocytes of 572 total, $n_{T.\ gondii} = 39$ transmigrated monocytes of 419 total from 7 independent experiments.

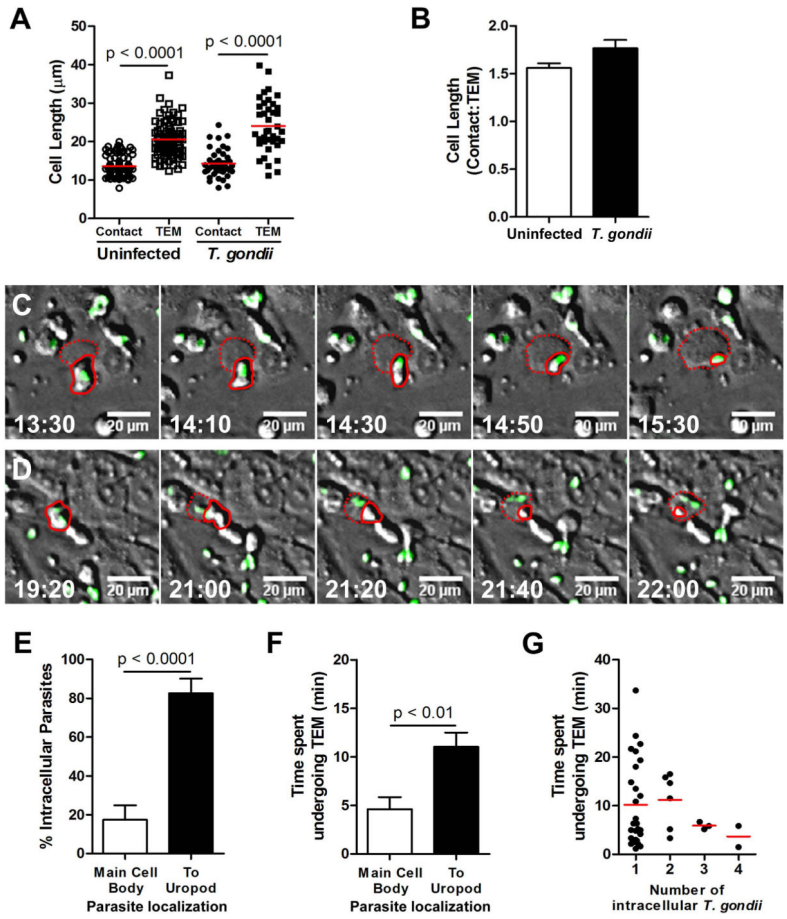

Figure 3.

Monocyte morphology and parasite localization during TEM of *T. gondii*-infected monocytes. (A) The cell length of each monocyte during initial contact with the endothelium and during TEM was measured. Red lines represent the means. (B) The change in cell length was calculated as a ratio of cell length at the point of first contact with endothelium to the length during TEM. Bars represent the mean ± SEM. (C and D) Infected monocyte TEM during which the GFP^+ parasites localized to the uropod (C) or remained in the main cell body (D) were imaged in real-time using DIC and fluorescence microscopy. Solid red lines indicate the portion of the cell above the endothelium. Dotted red lines indicate the portion of the cell below the endothelium. GFP^+ parasites are shown in green. Time stamps indicate min:sec after monocyte contact with the endothelium. Representative cells from 7 independent experiments are shown. (E) Percent intracellular parasites localized in the main cell body or in the uropod during TEM was quantified relative to the total number of infected monocytes that underwent TEM. Bars represent the mean ± SEM. (F) Time spent undergoing TEM was quantified for monocytes with parasites localized in the main cell body or in the uropod during TEM. Bars represent the mean ± SEM. (G) Time spent undergoing TEM was plotted for each monocyte based on the number of intracellular parasites within. Red lines represent the mean. For A, B, E-G, $n_{uninfected} = 83$, $n_{T.\ gondii} = 39$ from 7 independent experiments.

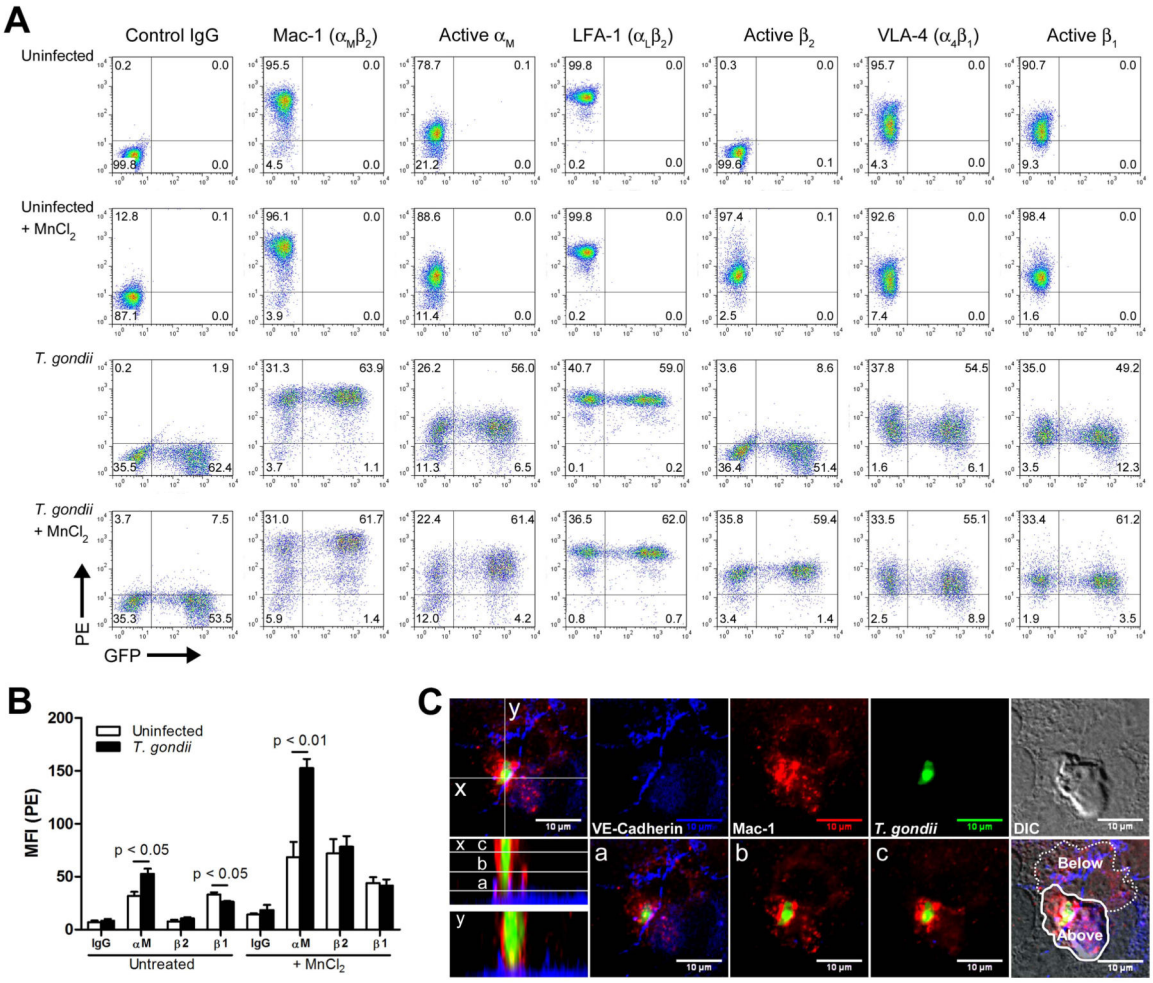

Figure 4.

Expression, activation, and localization of integrins on *T. gondii*-infected monocytes. (A) Uninfected monocytes or GFP$^+$ *T. gondii*-infected monocytes with or without Mn^{2+} stimulus were stained with mAb for total Mac-1, LFA-1, VLA-4, integrin, or the active form of the α_M, β_2, or β_1 integrin subunits and analyzed by flow cytometry. (B) Uninfected or *T. gondii*-infected monocytes were stimulated with Mn^{2+} or left untreated and subsequently stained for active α_M, β_2, or β_1, integrin subunits. Bars represent the average MFI ± SEM from 3 independent experiments. (C) Monocytes were infected with GFP$^+$ *T. gondii* and settled on HUVEC monolayer. After 1 h, the samples were fixed and stained for Mac-1 on the monocytes and VE-cadherin on the HUVEC. Monocytes that had started but not fully completed TEM were imaged by confocal microscopy. Top row: projection of the fluorescent z-stack and a DIC image focused at the top surface of the HUVEC, showing the portion of the monocyte above the monolayer. Bottom row: orthogonal x- and y-slices reconstructed from the z-sections and an accompanying merged image, made from overlaying the fluorescent and DIC images. Solid and dotted white lines in the merged image indicate the portions of the cell above and below the endothelium, respectively. For A and C, representative data from 3 independent experiments are shown.

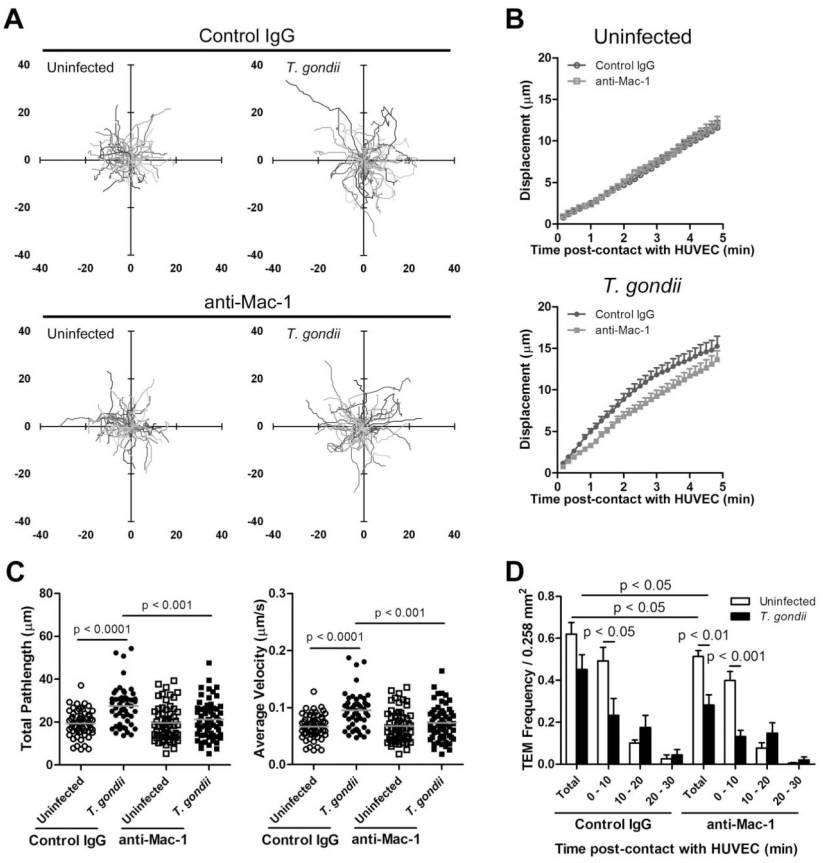

Figure 5.

Mac-1-mediated crawling and transmigration by uninfected and *T. gondii*-infected monocytes under fluidic shear stress. Infected monocytes were treated with control IgG or anti-Mac-1 function-blocking mAb and flowed into a fluidic channel lined with HUVEC at 0.5 dyn/cm^2. (A) Motility plots for each monocyte were generated using cell tracking data from the initial 5 min of crawling. The axes show the distance in μm. The direction of flow is from left to right. (B) Monocyte crawling displacement from the origin following control IgG versus anti-Mac-1 mAb treatment was plotted with respect to time post-contact with endothelium. Data points represent the mean ± SEM. The slopes of the lines are significantly different for *T. gondii*-infected monocytes ($p < 0.05$), but not for uninfected monocytes. (C) Crawling was quantified for each monocyte by calculating the total pathlength and average velocity for 5 min. Gray lines represent the mean. (D) TEM frequency was quantified from time-lapse micrographs, normalized for the area of the field of view, and further characterized based on the time spent crawling by the monocyte prior to TEM. Bars represent the mean ± SEM. For A-C, $n_{\text{IgG uninfected}} = 60$, $n_{\text{IgG } T.\ gondii} = 50$, $n_{\text{anti-Mac1 uninfected}} = 60$, $n_{\text{anti-Mac-1 } T.\ gondii} = 60$ from 8 fields of view from 2 independent experiments. For D, $n_{\text{IgG uninfected}} = 134$ transmigrated monocytes of 209 total, $n_{\text{IgG } T.\ gondii} = 27$ transmigrated monocytes of 69 total, $n_{\text{anti-Mac-1 uninfected}} = 201$ transmigrated monocytes of 367 total, $n_{\text{anti-Mac-1 } T.\ gondii} = 41$ transmigrated monocytes of 109 total from 8 fields of view from 2 independent experiments.

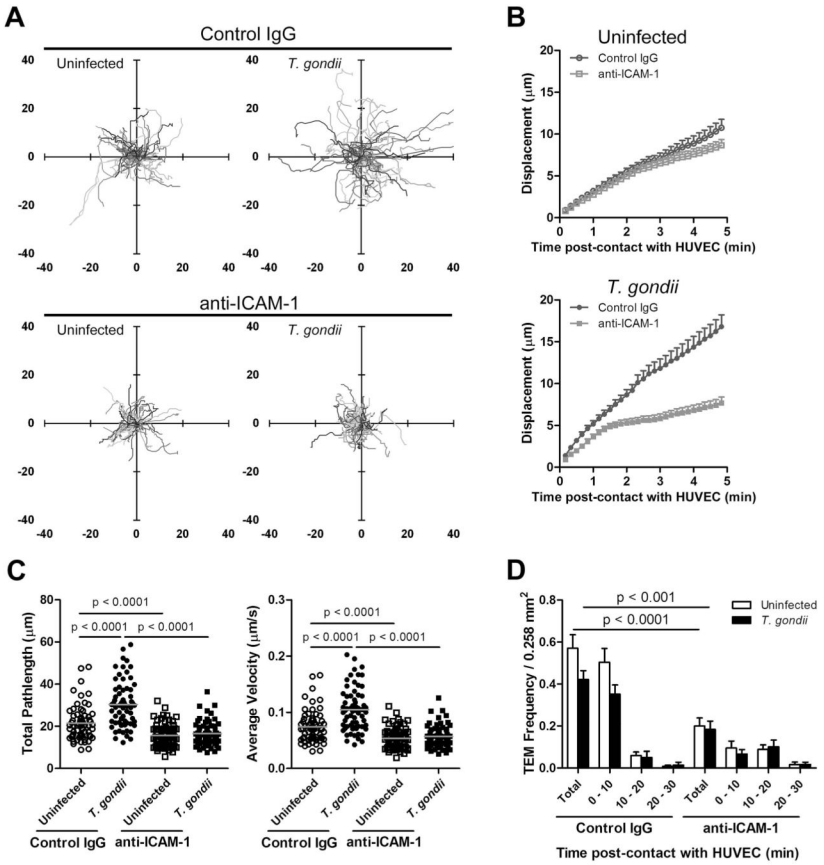

Figure 6.

ICAM-1-mediated crawling and transmigration by uninfected and *T. gondii*-infected monocytes under fluidic shear stress. HUVEC monolayers lining a fluidic channel were treated with control IgG or anti-ICAM-1 function-blocking mAb, and monocytes were flowed into the channel at 0.5 dyn/cm^2. (A) Motility plots for each monocyte were generated using cell tracking data from the initial 5 min of crawling. The axes show the distance in μm. The direction of flow is from left to right. (B) Monocyte crawling displacement from the origin following control IgG versus anti-ICAM-1 mAb treatment was plotted with respect to time post-contact with endothelium. Data points represent the mean ± SEM. For both uninfected and *T. gondii*-infected monocytes, the slopes of the lines are significantly different ($p < 0.0001$). (C) Crawling was quantified for each monocyte by calculating the total pathlength and average velocity for 5 min. Gray lines represent the mean. (D) TEM frequency was quantified from time-lapse micrographs, normalized for the area of the field of view, and further characterized based on the time spent crawling by the monocyte prior to TEM. Bars represent the mean ± SEM. For A-C, $n_{\text{IgG uninfected}} = 66$, $n_{\text{IgG } T.\ gondii} = 66$, $n_{\text{anti-ICAM-1 uninfected}} = 70$, $n_{\text{anti-ICAM-1 } T.\ gondii} = 70$ from 12 fields of view from 3 independent experiments. For D, $n_{\text{IgG uninfected}} = 102$ transmigrated monocytes of 178 total, $n_{\text{IgG } T.\ gondii} = 34$ transmigrated monocytes of 89 total, $n_{\text{anti-ICAM-1 uninfected}} = 30$ transmigrated monocytes of 175 total, $n_{\text{anti-ICAM-1 } T.\ gondii} = 17$ transmigrated monocytes of 89 total from 12 fields of view from 3 independent experiments.

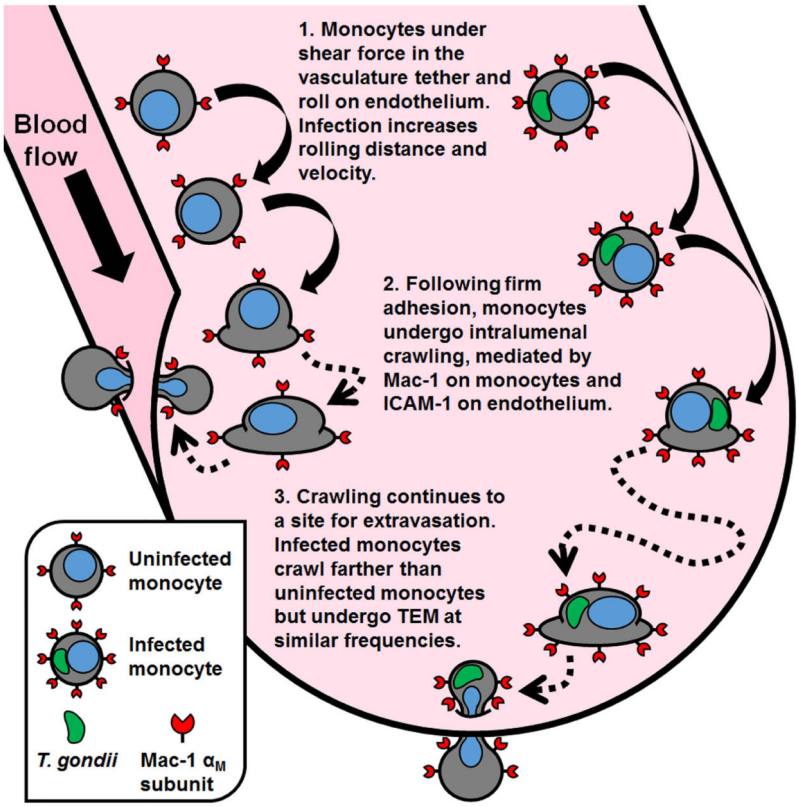

Figure 7.

A model for uninfected and *T. gondii*-infected monocyte extravasation. (1) Monocytes in the bloodstream tether to the blood vessel wall due to selectin-selectin ligand interactions, which bring the monocyte in close proximity to the endothelium and initiate rolling. During rolling, chemokine receptor signaling in the monocyte increases the affinity of monocyte surface integrins for their ligands, such as ICAM-1. Compared to uninfected monocytes, infected monocytes roll over longer distances before coming to arrest. This may be due in part to parasite-induced changes in the distribution of surface integrins (Harker *et al.*, 2013, Weidner *et al.*, 2013), which could delay firm adhesion to the endothelium. (2) After slow rolling, monocytes firmly adhere and begin crawling on the endothelial surface. Whereas uninfected cells perform short-distance intralumenal crawling and quickly arrive at a site of TEM, infected cells crawl for a longer period of time and migrate farther from their point of origin, a process that is mediated by the integrin Mac-1 and its ligand ICAM-1. Infected cells express a higher level of the high-affinity conformation of Mac-1 than uninfected monocytes. (3). Monocyte TEM is a rapid process that lasts only minutes, but infection may prolong this process, potentially due to the physical constraints of translocating intracellular parasites across the endothelial barrier. As with crawling, monocyte TEM is mediated by Mac-1 or ICAM-1.